To Appear in ApJS
Preprint typeset using LaTeX style emulateapj v. 10/09/06

ZBOÖTES : Z-BAND PHOTOMETRY IN THE NOAO DEEP WIDE-FIELD SURVEY BOÖTES FIELD

Richard J. Cool[1]

To Appear in ApJS

ABSTRACT

We present *z*Boötes, a new *z*-band photometric imaging campaign of 7.62 square degrees in the NOAO Deep Wide-Field Survey (NDWFS) Boötes field. In this paper, all of the images for this survey are released as well as the associated catalogs. The final *z*Boötes catalogs are complete (at the 50% level) to 22.7 mag over 50% of the field. With these depths, the *z*Boötes images should be sensitive to L^* galaxies to $z \sim 1$ over much of the survey area. These data have several possible applications including searching for and characterizing high-redshift quasars and brown dwarfs and providing added constraints to photometric redshift determinations of galaxies and active galaxies to moderate redshift. The *z*Boötes imaging adds photometric data at a new wavelength to the existing wealth of multi-wavelength observations of the NDWFS Boötes field.

Subject headings: catalogs, surveys, astronomical data bases:miscellaneous, galaxies:photometry

1. INTRODUCTION

In recent years, a number of multi-wavelength surveys have been completed in order to understand the evolution of the multi-wavelength properties of galaxies and active galactic nuclei (AGNs) throughout cosmic history. Deep observations spanning from the ultraviolet to the radio are time consuming and obtaining spectroscopic follow-up observations of cataloged galaxies and AGNs requires many nights on the largest telescopes available. Thus, the area covered by many of the deepest multi-wavelength surveys is fairly small. With the advent of new wide-field optical and near-infrared imagers and multi-object spectrographs, as well as superb new space facilities such as *GALEX* and *Spitzer*, the amount of the sky observed at all possible wavelengths is growing steadily.

One of the early deep, wide area, optical surveys, the NOAO Deep Wide-Field Survey [1] (NDWFS; Jannuzi et al. *in prep.*, Dey et al., *in prep.*) consists of two $\sim$ 9 square degree fields (the Boötes and Cetus fields) with excellent optical (B_W, R, and I) and near-infrared (K_s) photometry. The NDWFS Boötes field has become a popular target for many investigators and now has been observed across the full electromagnetic spectrum. Deep GALEX pointings provide near and far-ultraviolet photometry for the field; the NDWFS images consist of optical and near-infrared coverage, and the FLAMINGOS Extragalactic Survey (FLAMEX; Elston et al. 2005) observed the field to deep limits in J and K_S. *Spitzer* has imaged the Boötes field with both IRAC (Eisenhardt et al. 2004, Spitzer Shallow Survey;) and MIPS. Radio observations include deep Westerbork observations at 1.4 GHz (de Vries et al. 2002) and imaging by the Faint Images of the Radio Sky at Twenty-Centimeters survey (FIRST; Becker et al. 1995). *Chandra* has observed the Boötes field for 5 ksec (XBoötes; Murray et al. 2005; Kenter et al. 2005). Optical spectroscopy for several highly complete samples of galaxies and AGN has been completed with the Hectospec multi-object spectrograph on the MMT as part of the AGN and Galaxy Evolution Survey (AGES; Kochanek in prep). A small region in the Boötes field was observed as part of the LALA survey to search for galaxies at very high redshifts (Rhoads et al. 2000). These data sets have allowed searches for high-redshift quasars and low mass stars using mid-infrared selection techniques (Stern et al. 2006), studies of the quasar luminosity function (Brown et al. 2006; Cool et al. 2006), the clustering of high-redshift galaxies (Brown et al. 2005; Stanford et al. 2005; Rhoads et al. 2004; Brown et al. 2003), Lyman alpha emitting galaxies (Wang et al. 2004; Dey et al. 2005; Dawson et al. 2004; Rhoads et al. 2003), the broad band properties of AGNs (Brand et al. 2006, 2005; Stern et al. 2006, 2005), the X-ray properties of AGNs (Brand et al. 2006; Kollmeier et al. 2005), the spectral properties of infrared sources (Weedman et al. 2006; Desai et al. 2006; Khan et al. 2005; Higdon et al. 2005) and many other topics.

In this paper, we present new *z*-band observations of 7.6 square degrees in the NDWFS Boötes region. These catalogs reach several magnitudes deeper than the public imaging released by the Sloan Digital Sky Survey (SDSS) and will provide a useful intermediate photometric measurement between the I band data from NDWFS and near-infrared photometry from FLAMEX. We release the catalogs and reduced images for public use. Throughout this paper, all magnitudes are AB magnitudes (Oke 1974).

2. OBSERVATIONS

The *z*Boötes imaging survey was completed with the 90Prime wide-field imager (Williams et al. 2004) at prime focus on the Bok 2.3m Telescope located on Kitt Peak. This instrument consists of four 4096x4096 thinned CCDs, providing excellent quantum efficiency in the blue, read out using eight amplifiers. The chips are arranged in a windowpane pattern with 10' gaps between each of the CCDs. Each CCD images a 30'x30' field on the sky with 0.45" pixels. The south-east CCD has a large electron trap, making 13% of the area on that chip unusable for photometric measurements. These pixels

[1] Steward Observatory, 933 N Cherry Avenue, Tucson AZ 85721; rcool@as.arizona.edu

[1] http://www.archive.noao.edu/ndwfs
http://www.noao.edu/noao/noaodeep

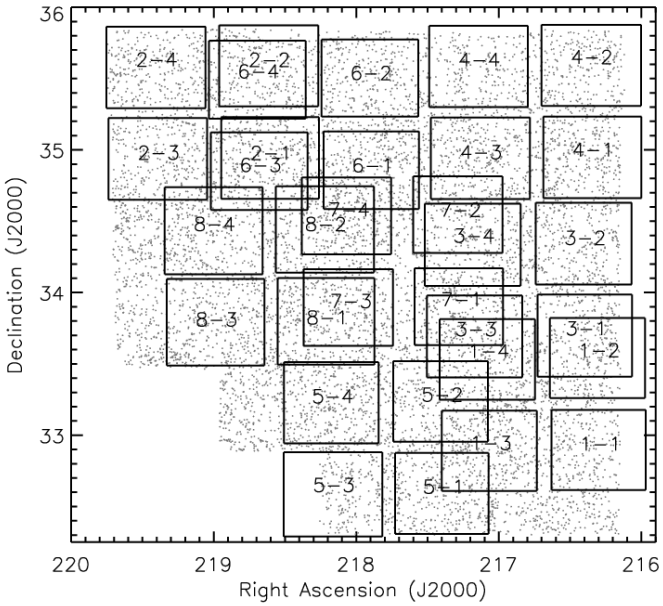

FIG. 1.— Map of the NDWFS survey area with the coverage of the *z*Boötes catalog overlayed. The grey points illustrate the distribution of 25% of the $I < 21.5$ galaxies in the NDWFS catalogs. Each of the subfields of the *z*Boötes imaging is labeled with the field number. The *z*Boötes imaging covers 7.6 square degrees centered on the NDWFS Boötes Field, providing another set of data to the current suite of multi-wavelength observations completed in this region.

are masked throughout the reduction process and are excluded when images are stacked.

The data were obtained between 28 Feb 2005 and 31 Mar 2005. Sky conditions varied from photometric to moderate levels of cirrus throughout the observations. The typical seeing during these observations was 1.6 arcsec. In total, we completed observations for eight 90Prime pointings within the NDWFS Boötes region. At each location, we obtained several dithered 300s exposures (typically 12 exposures per field). The telescope was moved $\sim 1'$ for each dither. The total number of exposures for each field was determined by the conditions at the time of the observations. All of the exposures for a single field were obtained on the same night. As the gaps between CCDs on 90Prime are rather large, we did not attempt to make our dither pattern large enough the fill the regions between each CCD. This strategy avoids having non-uniform depth across a single field but results in gaps in our photometric coverage of the NDWFS survey field. Figure 1 shows the region covered in the zBoötes survey compared to the NDWFS Boötes Survey area. Throughout the rest of this paper, each of the fields imaged by a single 90Prime CCD is treated independently.

3. REDUCTIONS

All of the raw *z*Boötes images were processed using a combination of home-grown IDL routines and various tasks available within the Image Reduction and Analysis Facility (IRAF). Each image was bias and overscan corrected and known bad columns are removed by interpolating neighboring columns. On each night of clear skies, observations of the twilight sky were taken to generate a flat field image that was divided into each object frame to correct for pixel-to-pixel variations in the CCD sensitivity.

While the thinned-chip nature of the CCDs on 90Prime allows for high efficiency in the blue, it also results in strong fringing in the reddest bands where the night sky spectrum is dominated by a forest of emission lines. On each night of observation, between 12 and 42 individual dithered images were obtained for this project in the z-band. To generate a master fringe frame, we first removed any large scale gradient in the background of each input image. The strength of the fringe pattern was then measured on each image and a multiplicative scale factor was applied to correct for any differences from the mean. We generated a master fringe frame by taking the median of all of the individual images taken on a single night of observations. This fringe frame was scaled to match the average strength of the fringes in each individual exposure and subtracted. This process was iterated (typically twice) until the fringe pattern was no longer present in each individual exposure. Figure 2 (a) and (b) shows a region of a single exposure before any processing and after the fringe pattern was been removed.

The astrometry of each image was calibrated by locating stars with $17 < z < 19$ from the Sloan Digital Sky Survey (SDSS) DR4 (Adelman-McCarthy et al. 2006). We fit the astrometric solution with a 5th order TNX world-coordinate system (WCS) using the IRAF task CCMAP. The images were then de-projected onto a rectilinear pixel system using the task MSCIMAGE in the MSCRED package in IRAF. Finally, aperture photometry of several stars in the magnitude range $17 < z < 19$ was performed on each of the input frames in order to determine offsets in the background level and photometric zeropoint between each of the frames. Any variations in the mean background or transparency were corrected before the individual images were stacked to create the final coadded frame for each field. Pixels with values more than 3σ from the mean were clipped when creating the final mosaic; this clipping rejected any cosmic rays present in the individual frames. Figure 2 shows a portion of a final stacked image.

The photometric zeropoint for each stacked image was determined by comparison with photometry publicly available from the SDSS (Adelman-McCarthy et al. 2006). Aperture photometry for stars with $18 < z < 19$ was compared to SDSS PSF magnitudes. The mean magnitude offset between the two photometric measurements was adopted as the magnitude zeropoint of the field. In general, the dispersion around this median was on the order of $\sigma_z \sim 0.03$ mag, comparable to the photometric scatter expected due to errors in the SDSS photometry (Ivezić et al. 2004). As the effective response of the z-band filter used in our work (including the effects of mirror reflectance and sky absorption) is likely different from that of the SDSS system, we examined the residuals between the *z*Boötes photometry and the SDSS photometry as a function of the SDSS $i-z$ color of each object. The photometric residuals showed no correlation with the object color, and thus no color term has been applied to the *z*Boötes photometry.

Several of the *z*Boötes fields overlapped significantly. These regions of significant overlap were coadded, weighted by seeing and signal-to-noise in each input frame, to create mosaiced images of the overlap regions. Before coadding the individual images in the overlap regions, each of the input images were background sub-

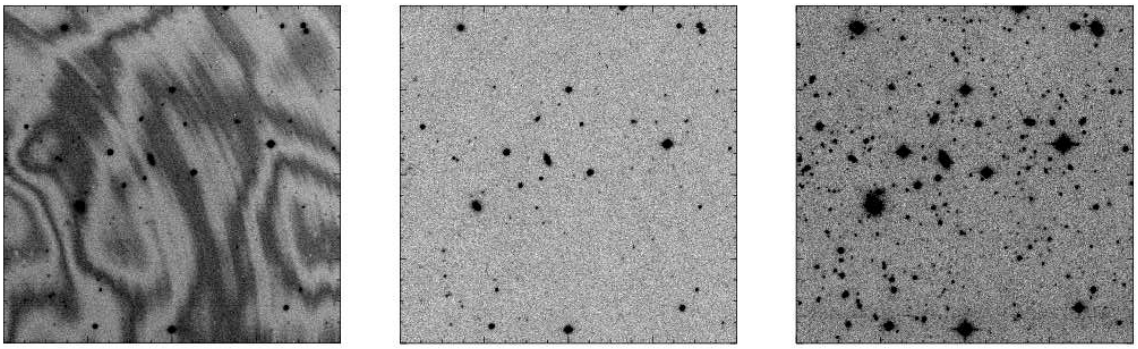

FIG. 2.— Example of the reduction steps performed on the *z*Boötes imaging data. Frame (a) shows a portion of a raw data frame taken with 90Prime. Frame (b) illustrates the same frame after flat-fielding and fringe correction. The final coadded frame, including all of the observations for this field, is shown in frame (c). Each of the images is 800 pixels on a side corresponding to ~ 6 arcminutes. The total exposure time for this field was one hour.

tracted and the measured counts per pixel were converted to a true flux density per pixel measurement using the photometric zeropoint determined from comparison with public SDSS photometry discussed above. Figure 3 illustrates the area of the *z*Boötes field included in these coadded observations compared to the object distribution in the NDWFS optical catalogs.

4. SOURCE CATALOGS

4.1. *Catalog Generation*

We constructed catalogs for each *z*Boötes field using Source Extractor (SExtractor) version 2.3 (Bertin & Arnouts 1996). We detected objects using a 0.9" FWHM Gaussian convolution kernel and enforced a 3σ detection threshold. Pixels were weighted according to the number of input exposures that contributed to each in order to prevent the detections of a large number of spurious sources around the edges of each field which have fewer average observations and thus higher background noise than the centers. For each object detected in the catalog, we measured the flux in ~ 100 apertures (with diameter 3", 5", and 7") in a 6 arcminute radius around the object. We used the interval containing 68.7% of the measurements as a measurement of the photometric error for each object. The simulated photometric errors we calculate from this method are about a factor of 2 larger than those measured by SExtractor.

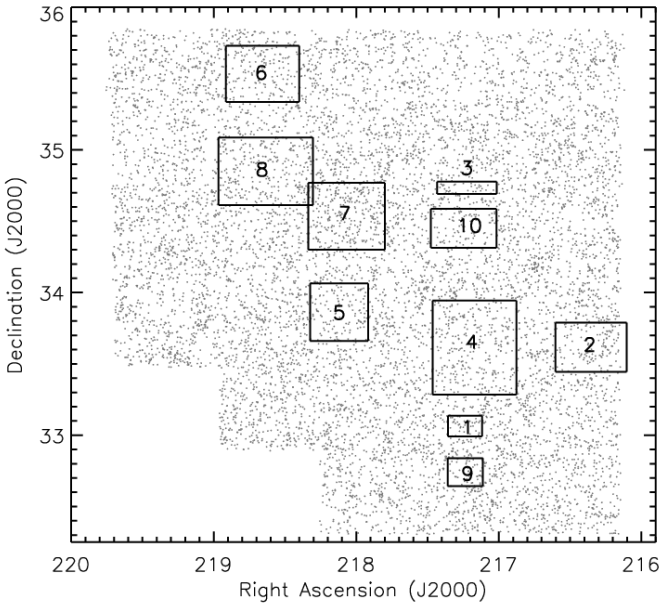

FIG. 3.— Map of the NDWFS survey area with the coverage of the coadded *z*Boötes fields overlayed. As in Figure 1, the grey points show the distribution of 25% of the $I < 21.5$ extended sources from the NDWFS catalogs. The number marking each of the coadded subfields denotes the field number assigned to that subfield. The coadded imaging covers 1.24 square degrees of the 7.62 square degree *z*Boötes region.

Catalogs were also constructed for each of the stacked images created for the overlapping *z*Boötes fields using the same process as used for individual subfields. The final *z*Boötes catalog was constructed by checking each object for duplicate observations. For any object that was observed multiply, we define the best observation to be the measurement with the smallest simulated photometric errors. The final *z*Boötes catalogs consists of over 200,000 objects.

Objects in the final *z*Boötes catalogs were matched to detections in the NDWFS catalogs (DR3). For each NDWFS subfield, we checked for systematic offsets in both right ascension and declination between the *z*Boötes astrometric system and the NDWFS reference frame. After removing any net offset between the NDWFS catalogs and our *z*Boötes catalogs (which are discussed in more detail in §4.3), the two object lists were matched with a 1" match tolerance and the name and coordinates of the closest match NDWFS detection were recorded in the final *z*Boötes catalog.

4.2. *Photometric Accuracy*

The final residuals between *z*Boötes and SDSS photometric measurements for well detected stars whose photometry is not affected by non-linearity in the 90Prime CCDS are centered around zero with a 1σ dispersion of 0.035 mag. The average quoted photometric error for the SDSS stars is 0.03 mag and thus the majority of the final calibration error in the *z*Boötes catalog can be attributed to photometric scatter in the SDSS photometry. The remainder of the scatter in the photometric calibration is likely due to errors in the large-scale flatfield corrections to each frame and imperfect subtraction of the strong fringing the 90Prime CCDs.

Since 1.25 square degrees were observed more than once in the *z*Boötes imaging, we can quantitatively estimate the error in our photometric measurements, both from calibration errors and reduction imperfections. The distribution of fluxes for the $\sim$ 7200 stars with $17 <$

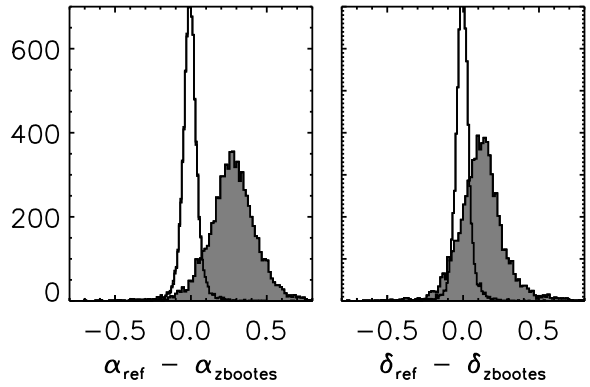

FIG. 4.— Histogram of astrometric offsets (in arcseconds) between sources reported by *z*Boötes and SDSS (unfilled) and *z*Boötes and NDWFS (filled). Only well-detected stars are used in this plot, so photon noise is not the dominant source of uncertainty in the astrometry. In general, SDSS and *z*Boötes agree quite well (50 mas rms). There are offsets between the *z*Boötes and NDWFS for each of the subfields, resulting in a overall mean offset and larger dispersion seen in the comparison between the *z*Boötes and NDWFS coordinates.

$z < 20$ observed two or more times within *z*Boötes itself has zero mean and a 1σ dispersion of 0.03 mag, in good agreement with the scatter in photometric calibration estimated above.

4.3. *Astrometric Precision*

As the *z*Boötes astrometry was calibrated to the SDSS reference system, the agreement between SDSS and *z*Boötes astrometry is quite good. Figure 4 shows the differences between SDSS, *z*Boötes , and NDWFS astrometry. The dispersion between the *z*Boötes and SDSS coordinates is ~ 50 milliarcsec (mas) per coordinate while the agreement with NDWFS is poorer with a dispersion of nearly 130 mas per coordinate. SDSS astrometry has a 45 mas dispersion per coordinate (Pier et al. 2003), so the *z*Boötes astrometric error is dominated by astrometric errors in the SDSS catalogs. Also, notice that the NDWFS and *z*Boötes astrometric have systematic offsets in both directions, likely due to the different astrometric reference systems used by NDWFS and SDSS imaging. Robust comparisons between NDWFS and *z*Boötes (or SDSS) thus require the removal of these offsets to properly match objects in each catalog. Table 1 lists the average shifts between the astrometry of each *z*Boötes field and the NDWFS catalog.

4.4. *Survey Depth*

The depth of the *z*Boötes images varies between each field and as a function of position in each field itself due to the variable number of exposures taken for each field and variable conditions during the observations. In order to quantify the depth of our catalogs near each detected object, we added fake point sources with the same point spread function as measured from nearby unsaturated stars in the *z*Boötes images. For each field, we perform ten simulations with each simulation consisting of 3000 fake stars added to the coadded frame of each field. We then record the average 50% completeness in a 10 arcminute diameter region around each object detected in our catalogs. Figure 5 illustrates the variations in the survey depth within a single *z*Boötes field. As illustrated in the figure, the variations in survey depth can be as large as 0.5 mags across the field.

TABLE 1
ASTROMETRIC OFFSETS BETWEEN *z*BOÖTES AND NDWFS

Field Name	$\Delta\alpha$ ″	$\Delta\delta$ ″	Field Name	$\Delta\alpha$ ″	$\Delta\delta$ ″
b1-1	-0.37	-0.31	b6-2	-0.25	-0.17
b1-2	-0.30	-0.37	b6-3	-0.31	-0.12
b1-3	-0.22	-0.18	b6-4	-0.24	-0.09
b1-4	-0.29	-0.15	b7-1	-0.22	-0.12
b2-1	-0.30	-0.05	b7-2	-0.26	-0.10
b2-2	-0.22	-0.04	b7-3	-0.28	-0.11
b2-3	-0.24	-0.08	b7-4	-0.30	-0.13
b2-4	-0.21	-0.09	b8-1	-0.35	-0.10
b3-1	-0.20	-0.13	b8-2	-0.37	-0.17
b3-2	-0.23	-0.10	b8-3	-0.26	-0.04
b3-3	-0.25	-0.15	b8-4	-0.33	-0.12
b3-4	-0.27	-0.13	mos-01	-0.17	-0.10
b4-1	-0.03	-0.05	mos-02	-0.25	-0.22
b4-2	-0.01	0.01	mos-03	-0.21	-0.10
b4-3	-0.11	-0.10	mos-04	-0.20	-0.17
b4-4	-0.11	-0.11	mos-05	-0.33	-0.11
b5-1	-0.17	0.02	mos-06	-0.21	0.07
b5-2	-0.30	-0.12	mos-07	-0.30	-0.12
b5-3	-0.20	0.08	mos-08	-0.32	-0.00
b5-4	-0.28	-0.18	mos-09	-0.13	0.04
b6-1	-0.32	-0.13	mos-10	-0.21	-0.07

Figure 6 shows the fraction of the *z*Boötes coverage area as a function of the 50% completeness depth and as a function of the 3σ detection limits of the catalogs. The final *z*Boötes catalog is 50% complete to 22.4 mag over 90% of the survey area and 50% of the survey area is complete to 22.7 mag. Thus, the *z*Boötes catalogs reach more than 2 mag fainter than SDSS over the entire survey region. The mosaiced images of the overlapping *z*Boötes fields reach fainter limits than the single frames.

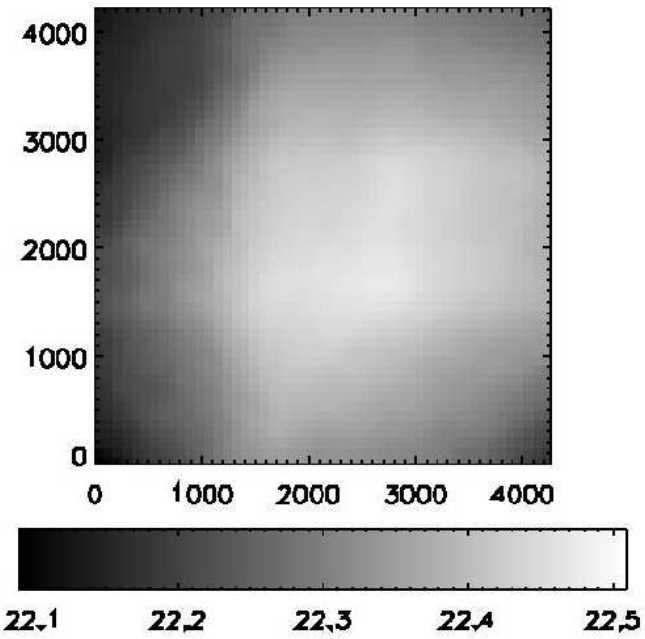

FIG. 5.— Map of the 50% completeness limit of the b4-1 field in pixel coordinates. The depth of the catalogs are a strong function of position in the final mosaiced image. This is primarily due to the decreased number of exposures that were coadded near the edge of the mosaiced field. The completeness can vary as much as 0.5 mag from the center of the field to the edge.

TABLE 2
Average Completeness Limits (50%) of *z*Boötes Fields

Field Name	Depth mag	Field Name	Depth mag
b1-1	22.35	b6-2	22.93
b1-2	22.50	b6-3	22.95
b1-3	22.54	b6-4	22.88
b1-4	22.52	b7-1	22.81
b2-1	22.59	b7-2	22.91
b2-2	22.68	b7-3	22.95
b2-3	22.79	b7-4	22.80
b2-4	22.72	b8-1	22.63
b3-1	22.56	b8-2	22.68
b3-2	22.69	b8-3	22.73
b3-3	22.67	b8-4	22.69
b3-4	22.63	mos-01	22.87
b4-1	22.58	mos-02	23.13
b4-2	22.50	mos-03	23.05
b4-3	22.76	mos-04	23.25
b4-4	22.63	mos-05	23.17
b5-1	22.39	mos-06	23.35
b5-2	22.48	mos-07	23.33
b5-3	22.46	mos-08	23.38
b5-4	22.41	mos-09	22.84
b6-1	22.85	mos-10	23.33

Note. — Depth is estimated by the 50% completeness limit of the catalogs.

Of the 1.24 square degrees covered in the overlapping fields, 50% of the area is complete to 23.3 mag and 90% is complete to 23.1 mag. Table 2 lists the average 50% completeness limit of each of the *z*Boötes subfields. The *z*Boötes data are thus sensitive to L^* galaxies to $z \sim 1$ and should provide extra constraint on photometric redshifts measurements for galaxies at $0 < z < 1$.

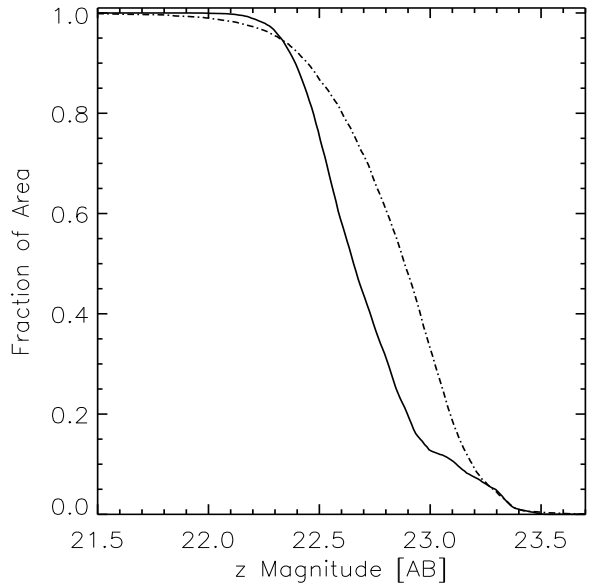

Fig. 6.— Fraction of the *z*Boötes survey area as function of the 50% completeness limit and 3σ detection limit of the *z*Boötes catalogs. The solid line shows the fraction of the *z*Boötes 7.6 square degree area as a function of the 50% completeness while the dot-dashed line shows the fraction of the survey area versus the 3σ detection limit in a 3 arcsecond aperture. The *z*Boötes catalog is complete to 22.4 mag over 90% of the survey area and 50% of the area is complete to 22.7 mag or deeper. The knee in the distribution of 50% completeness limit near $z = 23.0$ is due the deeper limits present in the coadded *z*Boötes fields as discussed in the text.

5. DATA PRODUCTS

5.1. *Images*

- Images and weight maps: `[fieldname.fits, fieldname-weight.fits]` We release the final coadded images and the associated weight map for each. The images are in ADU counts per pixel and the magnitude zeropoint of the photometry of each image is stored in the `MAGZERO` header keyword. The weight maps are normalized such that each pixel reflects the number of exposures that contributed to the image. All of these images have world-coordinate system information in the headers. Note that the orientation of these images corresponds to the orientation of the 90Prime images on the sky (north is to the right and east is upward) and not the standard image orientation.

  Regions of the sky that were observed in multiple *z*Boötes fields were coadded as described in §3. The resulting images are flux calibrated and have units of nano-maggies per pixel. A nanomaggie is a flux-density unit equal to 10^{-9} of a magnitude zero source. Since we calibrated the *z*Boötes photometry to SDSS, and SDSS is nearly an AB system, 1 nanomaggie corresponds to $3.631\,\mu$Jy or 3.631×10^{-29} erg s^{-1} cm^{-2} Hz^{-1}. As above, the weight maps associated with each of the mosaic images reports the total number of 300s exposures that contributed to each pixel.

- Photometric Catalogs: [`fieldname-cat.fits`] We also release binary FITS files of the SExtractor catalog for each *z*Boötes field as well as overlapping regions. In each file, we report the measured properties of each of the objects detected in the *z*Boötes imaging. A majority of the parameters listed in the catalogs are standard SExtractor outputs, so we will not repeat the definitions. The aperture fluxes and magnitudes reported in the *z*Boötes catalogs are measured at 12 diameters. The diameters run from 1" to 10" in steps of 1"; the final two apertures have diameters of 15" and 20". The non-standard parameters included in each of the catalogs are :

  - `NOBS` – [integer] Mean number of observations (300s exposures) that contribute to the pixels each object falls on. Objects with less than `NOBS` $\lesssim 5$ should be used with caution.
  - `ERR_[1,3,5,7]` – [float] Photometric error in a [1,3,5,7] arcsecond diameter aperture determined from the dispersion in the local sky background within a 6 arcminute radius around each object.
  - `COMP50` – [float] The 50% completeness limit determined by inserting $\sim 30,000$ fake point sources into the images and measuring the fraction recovered using the same analysis procedure as that used when constructing the catalogs. The local completeness is calculated within a 10 arcminute region around each object.
  - `DETECT_3SIG_3ARC` – [float] The local 3σ detection limit determined in a 3 arcsecond di-

ameter aperture around each object based on measurements of the local variation in the sky background.

– PHOTFLAG – [integer] For each object, this flag is set if any of the pixels contributing to the object detection were in the non-linear or saturated regime on the 90Prime CCDs. Photometry for objects with this flag set should be used with caution.

- Final Merged Catalog : [zbootes-cat.fits] The final catalog represents the merged catalog for the zBoötes imaging. For objects included in multiple individual catalogs, the observation with the smallest photometric error is declared the primary observation and included in the final catalog. Objects in the final catalog were cross-matched to the NDWFS optical catalogs using a 1 arcsecond search radius. Before the cross-matching was performed, the locally determined astrometric offsets between the zBoötes and NDWFS astrometric systems (reported in Table 1) were removed. The following parameters are included in the final catalog which are not in the individual catalogs:

  – FIELDNAME – [string] Name of the zBoötes field in which the photometric quantities for each object were measured.

  – DUPLICATE – [integer] Flag which is set if a given object was detected in multiple catalogs. If an object was detected in multiple frames, then the observation with the lowest photometric error was declared to be the best and included in the final merged catalog; each object is listed in the final catalog only once.

  – NDWFS_NAME – [string] Name of the nearest NDWFS object to each zBoötes detection. The catalogs were compared with a 1 arcsecond search radius; if there were no NDWFS objects within the search radius of the zBoötes object, this entry is empty.

  – NDWFS_RA – [double] Right ascension of the nearest NDWFS object to the zBoötes detection in decimal degrees.

  – NDWFS_DEC – [double] Declination of the nearest NDWFS object to the zBoötes detection in decimal degrees.

6. CATALOG AVAILABILITY

The zBoötes catalogs described in this paper are available for download online[2]. Any use of these data should include references to this paper. If any of the cross-identifications to the NDWFS catalogs are used, the appropriate citations should be made to the papers describing those data.

7. ACKNOWLEDGMENTS

RJC was funded through a National Science Foundation Graduate Research Fellowship. We are grateful to Ed Olszewski, Grant Williams, and Mike Lessar for providing the 90Prime instrument and technical information critical to the reduction and calibration of this data set. We thank Buell Jannuzi and Arjun Dey and the NOAO technical staff for hosting the data provided by this release. Daniel Eisenstein, Michael Brown, and Jane Rigby provided many useful comments and suggestions during the reduction and calibration of this dataset.

[2] http://archive.noao.edu/nsa/zbootes.html

REFERENCES

Adelman-McCarthy, J. K., et al. 2006, ApJS, 162, 38
Becker, R. H., White, R. L., & Helfand, D. J. 1995, ApJ, 450, 559
Bertin, E., &Arnouts, S. 1996, A&AS, 117, 393
Brand, K., et al. 2005, ApJ, 626, 723
Brand, K., et al. 2006, ApJ, 644, 143
Brand, K., et al. 2006, ApJ, 641, 140
Brown, M. J. I., Dey, A., Jannuzi, B. T., Lauer, T. R., Tiede, G. P., & Mikles, V. J. 2003, ApJ, 597, 225
Brown, M. J. I., Jannuzi,B. T., Dey, A., & Tiede, G. P. 2005, ApJ, 621, 41
Brown, M. J. I., et al. 2006, ApJ, 638, 88
Cool, R. J., et al. 2006, AJ, 132, 823
Dawson, S., et al. 2004, ApJ, 617, 707
Desai, V., et al. 2006, ApJ, 641, 133
Dey, A., et al. 2005, ApJ, 629, 654
Eisenhardt, P. R., et al. 2004, ApJS, 154, 48
Elston, R. J., et al. 2005, in press, arXiv:astro-ph/0511249
Higdon, J. L., et al.2005, ApJ, 626, 58
Ivezić, Ž., et al. 2004, Astronomische Nachrichten, 325, 583
Jannuzi, B. T., & Dey, A. 1999, ASP Conf. Ser. 191: Photometric Redshifts and the Detection of High Redshift Galaxies, 191, 111
Kenter, A., et al. 2005, ApJS, 161, 9
Khan, S. A., et al. 2005,ApJ, 631, L9
Kollmeier, J. A., et al. 2005, ArXiv Astrophysics e-prints, arXiv:astro-ph/0508657
Murray, S. S., et al. 2005, ApJS, 161, 1
Oke, J. B. 1974, ApJS, 27, 21
Pier, J. R., Munn, J. A., Hindsley, R. B., Hennessy, G. S., Kent, S. M., Lupton, R. H., & Ivezić, Ž. 2003, AJ, 125, 1559
Rhoads, J. E., Malhotra, S., Dey, A., Stern, D., Spinrad, H., & Jannuzi, B. T. 2000, ApJ, 545, L85
Rhoads, J. E., et al. 2003, AJ, 125, 1006
Rhoads, J. E., et al. 2004, ApJ, 611, 59
Stanford, S. A., et al. 2005, ApJ, 634, L129
Stern, D., et al. 2005, ApJ, 631, 163
Stern, D., et al. 2006, ArXiv Astrophysics e-prints, arXiv:astro-ph/0608603
Wang, J. X., et al. 2004, ApJ, 608, L21
Weedman, D. W., et al. 2006, ArXiv Astrophysics e-prints, arXiv:astro-ph/0606740
Williams, G. G.,Olszewski, E., Lesser, M. P., & Burge, J. H. 2004, Proc. SPIE,5492, 787
de Vries, W. H., Morganti, R., Röttgering, H. J. A., Vermeulen, R., van Breugel, W., Rengelink, R., & Jarvis, M. J. 2002, AJ, 123, 1784